Improved Hybrid Algorithm for Composite Scattering From Multiple 3D Objects Above a 2D Random Dielectric Rough Surface

GUILONG TIAN[ID][1]**, CHUANGMING TONG**[ID][1]**, HUALONG SUN**[1]**, GAOXIANG ZOU**[ID][1]**, AND HAO LIU**[2]

[1]Air and Missile Defense College, Air Force Engineering University, Xi'an 710038, China
[2]Troops 95899, Peoples' Liberation Army, Beijing 100085, China

Corresponding author: Guilong Tian (tianguilong163@163.com)

ABSTRACT In this paper, an improved hybrid scheme combining the method of moment (MoM) and physical optic (PO) is proposed to analyze composite scattering from multiple 3D conductingobjects above a 2D random rough dielectric surface. In the calculation scheme, rough surface scattering is calculated using the PO method and target scattering is calculated by the MoM. The coupling interactions between the multiple targets are considered using the domain distribution method (DDM), where the matrix equations are constructed upon each individual target and are then presented and solved as a whole. The contribution from rough surface scattering, which is calculated by the PO method, is coupled with the impedance matrix, and the unknowns must be considered only in the MoM region. Most of the composite scattering problems are computing interactions between objects and rough surface, and solving the complex impedance matrix equation in the MoM part. To solve these two problems, first, the combined multilevel fast multipole algorithm (MLFMA) and the fast far field approximation (FaFFA) are introduced to accelerate interactions between objects and rough surface, where the near area on the rough surface is computed by MLFMA, while the far area is computed by FaFFA. In addition, to further improve the efficiency, the adaptive integral method (AIM) is employed to solve the impedance matrix equation of the MoM part in the scheme. The results are compared to those obtained with the traditional MoM-PO method, showing that the hybrid method proposed in this paper can maintain a high accuracy with a much smaller computational time and fewer resource requirements. The numerical results obtained under several different conditions are presented and discussed in this paper.

INDEX TERMS Composite electromagnetic scattering, hybrid method, 3D multiple objects, 2D random rough dielectric surface.

I. INTRODUCTION

Composite scattering from multiple targets above a rough surface has been widely used in applications, such as navigation for multiple aircraft and detection of an important target among multiple targets in the air, and in other areas [1]–[6]. However, most studies of composite scattering reported in the literature only consider a single target above a rough surface. In contrast, the scattering properties for an environment with multiple targets have rarely been analyzed. This lack of studies is because the calculation of composite scattering

The associate editor coordinating the review of this manuscript and approving it for publication was Vittorio Degli-Esposti[ID].

from multiple targets above a rough surface must consider the complex interactions among different targets and the interactions between the targets and the rough surface. Moreover, as the number of targets increases, the evaluation of singular integrals becomes difficult. Among the studies of composite scattering from multiple targets with a rough surface reported in the literature, Ref. [7] studied composite scattering from multiple targets above and on a rough surface, and Ref. [8] computed composite scattering from multiple targets above and below a dielectric rough surface. Ref. [9] investigated wide-band composite electromagnetic scattering from a 1D dielectric surface and multiple shallow buried 2D conductor targets. Ref. [10] studied composite scattering from multiple

2D conductor spheres above a 1D rough conductor surface. Thus, all of these studies examined 2D multiple targets and a 1D rough surface. To the best of our knowledge, there have been rare reports considering composite scattering from three-dimensional (3D) multiple targets above a 2D random rough dielectric surface.

Numerical methods are typically used for composite scattering calculations. Among the numerical methods, the most common method is the method of moments (MoM) [11], which calculates the direct mutual effects between all the facets both on the object and on the rough surface. To accelerate the MoM, several improved numerical algorithms have been proposedsuch as the conjugate gradient method (CG) [12] the propagation-inside-layer expansion (PILE) [13], [14], the forward and backward algorithm [15] and the multilevel fast multipole method (MLFMM) [16]. Additionally, a method combining compressive sensing and the MoM [17] and a method based on compute unified device architecture (CUDA) [18] are used to further accelerate the MoM. However, these methods are not suitable for calculating composite scattering from electrically large targets above a rough surface because the computational complexity increases strongly with increasing numbers of unknowns in the composite model. Another class of methods that are typically used for composite scattering calculation is analytical methods such as the physical optics- physical optics (PO-PO) method [19]. However, pure analytical methods have become impractical for complex target shapes and numerous targets. Recently, numerical-analytical hybrid methods, such as MoM-PO [20], FE-BI-PO [21] and SPM/MoM [22] have been developed by combining the advantages of numerical and analytical methods; in this approach, analytical methods such as the PO method and the small perturbation method (SPM) are used to calculate scattering from a rough surface, and numerical methods such as the MoM are used to calculate scattering from the object. Compared to these models, MoM-PO is more efficient for calculating composite scattering from electrically large objects above a rough surfacebecause it only establishes the electric field integral equation (EFIE) on the surface of the object rather than inside the target. Two approaches have been used in the implementation of the MoM-PO hybrid schemes. The first is iterating the voltage matrix of the MoM with PO, and the second is coupling the contribution of the PO area into the impedance matrix of the MoM. For example, Ref. [23] used the iterative IEM–PO method to analyze composite scattering from a 2D PEC object above a 1D dielectric sea surface. In Ref. [24], Ye used the iterative KA-MoM technique to study scattering from a 3D target above a rough dielectric surface with the MoM part accelerated by using the conjugate gradient (CG) method. Among the studies using the fully coupled MoM-PO method, Ref. [20] analyzed composite scattering from a single 2D conductor target above a 1D rough sea surface. In Ref. [25], scattering from two conductor targets above a 1D rough surface was calculated, with scattering from the target and the rough surface treated as a whole.

Compared to the iterative MoM-PO technique, the fully coupled MoM-PO technique is more appropriate for calculating the scattering from multiple targets above a rough surface, because it considers all of the scattering interactions among the different targets and the scattering interaction between the targets and the rough surface, making this approach more accurate and enabling it to effectively avoid the problem of no convergence. Moreover, simulations have shown that when the length of the incident wave is similar to the roughness of the rough surface, the fully coupled MoM-PO technique is more suitable for solving scattering from the composite model as a whole [20].

However, for traditional fully coupled MoM-PO, as the number of targets increases, the PO area becomes larger, and the number of unknowns on the MoM area increases strongly, resulting in increasing computational cost for vector-matrix multiplications between the target and the rough surface as well as greater complexity of the impedance matrix of the MoM. To overcome the bottlenecks of the traditional MoM-PO technique for calculating scattering from multiple targets above a rough surface, acceleration strategies must be considered. In Ref. [26] and [27], the fast far field approximation (FaFFA) is presented to accelerate vector-matrix multiplication between the source group and field group. However, in the FaFFA scheme, the near field area is still computed by direct interaction, which requires long computing times. To further improve the efficiency, the combined MLFMA and the FAFFA technique is introduced [28]. In the combined MLFMA-FaFFA scheme, when distances between the object and rough surface do not meet the far field condition, interactions are accelerated by MLFMA, otherwise, the interactions are accelerated by FaFFA. Thus, the computing complexity can be significantly reduced. Furthermore, the surface truncation technique could be applied to reduce the computational area in the rough surface [29]. In addition, to solve the great complexity of the impedance matrix, the adaptive integral equation method (AIM) is effectively applied [30], with which the near area is computed directly, while the far area is accelerated with fast Fourier transform (FFT).

The paper is organized as follows: the traditional MoM-PO technique is discussed in Section II, theacceleration techniques are given in Section III, the rough surface model is introduced in Section IV, and the numerical results are presented in Section V, followed by the conclusions.

II. MOM-PO HYBRID METHOD

The setup of the system of multiple conductor targets above a rough surface is shown in Figure 1, where S_{tk}^{mom} is the target k in the MoM area, and S_r^{PO} is the rough surface in the PO area with a size of $L_x \times L_y$. The incident direction is denoted by $\boldsymbol{k}_i$, and the incident angle is (θ_i, φ_i). ε_r is the relative dielectric constant of the rough surface S_r^{PO}. The procedure used for the composite scattering calculation is as follows. (1) First, the scattering electric field from each target is expressed by the electric expansion coefficient. (2) Then, the scattering electric field acting as the incident field travels
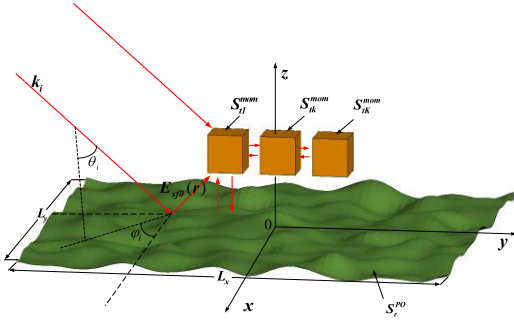
FIGURE 1. Schematic illustration of multiple objects above a rough surface.

from the target's surface to the rough surface, and the electric and magnetic fields induced on the PO area are obtained according to the scattering field from the targets and the outer incident field. (3) Finally, electric field integral equations (EFIEs) are constructed on the surface of each target, the contribution of the PO area is coupled into the impedance matrix of the MoM part, and the electric expansion coefficient is obtained by solving the EFIE; then, the total scattering field is obtained. For the MoM-PO method, unknowns are only required in the MoM area, greatly reducing the storage requirements. Furthermore, this approach considers all of the scattering contributions from the targets and the rough surface, guaranteeing the accuracy of this method. To ensure computational accuracy, the wavelength of the incident field must be less than the radius of curvature at the object surface.

A. SCATTERING FROM OBJECTS

The Rao-Wilton-Glisson (RWG) vector basic function is used to simulate the current distribution on the target. The surface of the targets k is represented by a mesh of N_k triangular facets. The electric currents on the facets of the target S_{tk}^{mom} excited by the incident field are J_{tk}. The expression for J_{tk} is

$$J_{tk} = \sum_{n=1}^{N_k} \alpha_{kn} f_{kn}, \quad k = 1, 2 \ldots K \tag{1}$$

where α_{kn} is the electric current expansion coefficient on the facets of the target S_{tk}^{mom}. The electric field excited by the induced electric currents in free space is

$$E_{tk}^s = L^e(J_{tk}), \quad k = 1, 2 \ldots K \tag{2}$$

where L^e is

$$L^e(J(r')) = ik\eta \int_S (\bar{\bar{I}} + \frac{\nabla \nabla'}{k^2})J(r')g(r,r')ds' \tag{3}$$

where $\bar{\bar{I}}$ is the unit parallel vector, $k = \omega\sqrt{\mu_0 \cdot \varepsilon_0}$ is the wavenumber in free space, $g(r,r') = e^{-jk|r-r'|}/4\pi|r-r'|$ is Green's function in free space, and $J(r')$ is the induced electric current. The scattering electric field on the target region is

$$E_t^s = \sum_{k=1}^K E_{tk}^s = \sum_{k=1}^K \sum_{n=1}^{N_k} \alpha_{kn} L^e(f_{kn}) \tag{4}$$

B. SCATTERING FROM A ROUGH SURFACE

According to the Huygens principle, when the incident field is E_i, the scattering electric field $E_s(r)$ from a rough surface is

$$E_s(r) = K^e(J_S(r), M_S(r))$$
$$= \int_s ds' \cdot ik\eta(\bar{\bar{I}} + \frac{\nabla \nabla'}{k^2})g(r',r) \cdot J_S(r)$$
$$+ \int_s ds' \nabla g(r',r) \times M_S(r) \tag{5}$$

When the local incident angle θ_i on the rough surface meets the condition $\cos\theta_i = -\hat{n} \cdot k_i$, for which the local orthogonal coordinate system $(\hat{p}, \hat{q}, \hat{k})$ is constructed, the horizontal and vertical polarization vectors are defined as

$$\hat{q} = \frac{k_i \times \hat{n}}{|k_i \times \hat{n}|}, \quad \hat{p} = \hat{q} \times \hat{k} \tag{6}$$

When the curvature radius ρ of a rough surface and the incident wavelength λ meet the condition $\rho \gg \lambda$, the condition of the tangent plan approximation is satisfied. Based on the tangent plan approximation, the local reflection direction is $\hat{k}_r = \hat{k}_i - 2\hat{n}(\hat{n} \cdot k_i)$, and the local reflected electric field and magnetic fields meet the condition of the TEM right-hand screw relationship.

The directly induced electric currents $J_{S0}(r)$ and the magnetic currents $M_{S0}(r)$ excited by the incident field E^{inc} on the rough surface are

$$J_{S0}(r)$$
$$= \hat{n} \times \left\{ \frac{(\hat{p} \cdot E^{inc})}{\eta}(1+R^{TM})\hat{q} - \frac{(\hat{q} \cdot E^{inc})}{\eta}[\hat{p} - R^{TM}\hat{k}_r \times \hat{q}] \right\}$$
$$M_{S0}(r)$$
$$= \hat{n} \times \left\{ (1+R^{TE})(\hat{q} \cdot E^{inc})\hat{q} + (\hat{p} \cdot E^{inc})[\hat{p} - R^{TM}\hat{k}_r \times \hat{q}] \right\} \tag{7}$$

where R^{TE} and R^{TM} are the Fresnel reflection coefficients under the condition of the local tangent plane approximation. $E_1(r)$ and $H_1(r)$ are generated by the outer incident field E^{inc}. $\hat{n}$ is the local outer normal vector. The induced electric currents $J_{Sd}(r)$ and magnetic currents $M_{Sd}(r)$ on the rough surface excited by the scattering field E_{tk}^s are

$$J_{Sd}(r)$$
$$= \hat{n} \times \left\{ \frac{1}{\eta}(\hat{p} \cdot E_t^s)(1+R^{TM})\hat{q} - \frac{1}{\eta}(\hat{q} \cdot E_t^s)[\hat{p} - R^{TM}\hat{k}_r \times \hat{q}] \right\}$$
$$M_{Sd}(r)$$
$$= \hat{n} \times \left\{ (1+R^{TE})(\hat{q} \cdot E_t^s)\hat{q} + (\hat{p} \cdot E_t^s)[\hat{p} - R^{TM}\hat{k}_r \times \hat{q}] \right\} \tag{8}$$

The total electric and magnetic currents on the rough surface are

$$J_S(r) = J_{Sd}(r) + J_{S0}(r)$$
$$M_S(r) = M_{Sd}(r) + M_{S0}(r) \tag{9}$$

The scattering electric field $E_s(r)$ from the rough surface to the targets can be expressed as

$$E_s(r) = E_{s0}(r) + E_{sd}(r)$$
$$= K^e(J_{s0}, M_{s0}) + K^e(J_{sd}, M_{sd}) \quad (10)$$

where $E_{s0}(r)$ is the direct scattering electric field from the rough surface, and $E_{sd}(r)$ is the mutual scattering electric field between the targets and the rough surface.

C. MUTUAL INTERACTION

The scattering field $E^S(r_k)$ from the target S_k^{mom} is composed of the contribution from the scattering electric field excited by the induced electric currents on the target itself, the electric currents induced on other targets and the electric and magnetic currents induced on the rough surface. The expression for $E^S(r_k)$ is

$$E^S(r_k) = L^e(J_{tk}) + \sum_{i=1,i\neq k}^{K} L^e(J_{ti}) + K^e(J_S, M_S) \quad (11)$$

When the incident wave is vertically polarized, based on the Dirichlet boundary condition, theEFIEfor the facets of the conductor target is

$$E_{\tan} = E^{inc} + E^S\big|_{\tan} = 0 \quad (12)$$

where E^{inc} is the outer incident electric field, and E^S is the scattering electric field in free space that is composed of the scattering electric field from the induced currents on the target and the rough surface. By substituting Eq. (11) into Eq. (12), Eq. (12) can be rewritten as

$$0 = \sum_{i=1,i\neq k}^{K} L^e[J_{ti}(r_i')] + K^e[J_{S0}(r_k'), M_{S0}(r_k')]$$
$$+ K^e[J_{Sd}(r_s'), M_{Sd}(r_s')]\big|_{\tan} + E^{inc}(r_s') + L^e[J_{tk}(r_s')],$$
$$(r_s' \in S_r^{po} \, r_k \in S_k^{mom}, k = 1, 2 \ldots K) \quad (13)$$

The equation is then tested by the Galerkin method and discretized as a matrix equation:

$$-\Big\langle L^e[J_{t1}(r_1')] + \sum_{i=2}^{K} L^e[J_{ti}(r_i')] + K^e[J_{Sd}(r_s'), M_{Sd}(r_s')], f_{1m}\Big\rangle_{\tan}$$
$$= \Big\langle E^{inc}(r_1'), f_{1m}\Big\rangle_{\tan} + \Big\langle K^e[J_{s0}(r_s'), M_{s0}(r_s')], f_{1m}\Big\rangle_{\tan}$$
$$\cdots$$
$$-\Big\langle L^e[J_{tk}(r_k')] + \sum_{i=1,i\neq k}^{K} L^e[J_{ti}(r_i')]$$
$$+ K^e[J_{Sd}(r_s'), M_{Sd}(r_s')], f_{km}\Big\rangle_{\tan}$$
$$= \Big\langle E^{inc}(r_k'), f_{km}\Big\rangle_{\tan} + \Big\langle K^e[J_{s0}(r_s'), M_{s0}(r_s')], f_{km}\Big\rangle_{\tan}$$
$$\cdots$$
$$-\Big\langle L^e[J_{tK}(r_K')] + \sum_{i=1}^{K-1} L^e[J_{ti}(r_i')]$$

$$+ K^e[J_{Sd}(r_s'), M_{Sd}(r_s')], f_{Km}\Big\rangle_{\tan}$$
$$= \Big\langle E^{inc}(r_K'), f_{Km}\Big\rangle_{\tan} + \Big\langle K^e[J_{s0}(r_s'), M_{s0}(r_s')], f_{Km}\Big\rangle_{\tan}$$
$$(r_s' \in S_r^{po}, r_k \in S_k^{mom}, k = 1,2\ldots K) \quad (14)$$

where the inner product of the vector is defined as $\langle f, g \rangle = \int_s f \cdot g \, ds$. This equation can be simplified as

$$\big[Z_{mn}^1 + Z_{mn}^{1t} + Z_{mn}^{1S}\big] \cdot [\alpha_1] = \big[V_1^{inc} + V_1^S\big]$$
$$\cdots$$
$$\big[Z_{mn}^k + Z_{mn}^{kt} + Z_{mn}^{kS}\big] \cdot [\alpha_k] = \big[V_k^{inc} + V_k^S\big]$$
$$\cdots$$
$$\big[Z_{mn}^K + Z_{mn}^{Kt} + Z_{mn}^{KS}\big] \cdot [\alpha_K] = \big[V_K^{inc} + V_K^S\big] \quad (15)$$

where Z_{mn}^k is the self-impedance matrix on the target S_{tk}^{mom}, Z_{mn}^{kt} is the mutual-impedance matrix between the target S_k^{mom} and the other targets, and Z_{mn}^{kS} is the mutual-impedance matrix between the targets and the rough surface. V_m^{inc} is excitation from the outer incident field, and V_m^S is excitation due to the interaction between the rough surface and the incident field.

The bistatic scattering coefficient (BCS) can be expressed as

$$\sigma_{\alpha\beta} = \lim_{r\to\infty} \frac{4\pi r^2 \left|E_\alpha^{Sur} + E_\alpha^{Tar}\right|^2 \cos\theta_i}{\left|E_\beta^i\right|^2 \cdot S \cdot \cos\theta_i} \quad (16)$$

where α is the scattering direction; β is the incident direction; E_α^{Sur} and E_α^{Tar} are the $\alpha-$ polarized scattering electric fields of the rough surface and the targets, respectively; E_β^i is the $\beta-$ polarized incident electric field; θ_i is the incident angle; and $S \cdot \cos\theta_i$ is the projected area that is illuminated by the incident wave in the direction of vertical polarization. The BCS can be obtained after the electric currents are induced on the targets and the electric and magnetic currents on the rough surface are calculated.

III. MODIFICATIONS AND ACCELERATION TECHNIQUES

A. FAFFA-MLFMA ACCELERATION TECHNIQUES

In Eq. (15), Z_{mn}^{kS} denotes the mutual-impedance matrix between objects and rough surfaces, which is obtained by vector-matrix multiplications between objects and rough surfaces. The computational complexity of Z_{mn}^{kS} is $O(2M^2P)$ [31], where M and P denote the number of basic functions in the MoM-region and the PO-region, respectively. Apparently, Z_{mn}^{kS} is time-consuming for an electrically large PO-region. To accelerate the vector-matrix multiplications, the multilevel fast multipole algorithm(MLFMA) and the fast far field approximation (FaFFA) are introduced.

1) MLFMA Algorithm

To operate the MLFMA and FaFFA algorithms, first, the model of 3D multiple objects is immersed in the smallest box that refers to the level zero. The zero-th box is then divided into eight subboxes, which are referred to the first

level. Each first level box is divided into eight boxes that are located in the second level. The procedure is recursively continued until the finest level L_f and the size of the box in this level are approximately $0.2\lambda \sim 0.5\lambda$. Thus, an oct-tree structure is made with the above procedure. Similarly, a quad-tree structure is made for rough surfaces. With the tree structure made, boxes at each level are indexed, and only the no-empty boxes are recorded.

The multilevel fast multipole algorithm (MLFMA) is based on the addition theorem. Suppose that $\boldsymbol{r}_m$ and $\boldsymbol{r}_{m'}$ are the center vectors of the field group and source group, respectively. $\boldsymbol{r}_a$ and $\boldsymbol{r}_b$ are the field point and source point, respectively, and $\boldsymbol{r}_{ab} = \boldsymbol{r}_a - \boldsymbol{r}_b = \boldsymbol{r}_{am} + \boldsymbol{r}_{mm'} - \boldsymbol{r}_{bm'}$. When the distance meets the condition $|\boldsymbol{r}_{mm'}| > |\boldsymbol{r}_{am} - \boldsymbol{r}_{bm'}|$, the Green function defined on the Ewald sphere can be expressed as [32]

$$\frac{e^{ik|\boldsymbol{r}_{ab}|}}{|\boldsymbol{r}_{ab}|} = \frac{ik}{4\pi} \int_{S_E} d^2\hat{\boldsymbol{k}} e^{-j\boldsymbol{k}\cdot(\boldsymbol{r}_{am}-\boldsymbol{r}_{bm'})} \alpha_{mm'}(\hat{k} \cdot \boldsymbol{r}_{mm'}) \quad (17)$$

where $\int_{S_E} d^2\hat{\boldsymbol{k}}$ denotes the integral on the unit sphere, the Ewald sphere. $\alpha_{mm'}(\hat{k} \cdot \boldsymbol{r}_{mm'})$ is the translator from the center of the field group to the center of the source group, and it can be expressed as follows:

$$\alpha_{mm'}(\hat{k} \cdot \boldsymbol{r}_{mm'}) = \sum_{i=0}^{L} (-j)^l (2l+1) h_l^{(1)}(kr_{mm'}) P_l(\hat{k} \cdot \hat{r}_{mm'})$$
$$(18)$$

where $h_l^{(1)}$ is the spherical Hankel function of the first kind, P_l is the Legendre polynomial, and L is the transaction number of infinite summation. According to Ref. [33]

$$L = \text{int}\left[kD_0 + 1.8d_0^{2/3}(kD_0)^{1/3}\right] \quad (19)$$

where D_0 is the largest group size. $d_0 = \log(1/\varsigma)$ denotes the required accuracy, and ς is the transaction error; generally, $\varsigma \le 10^{-3}$. The total sampling numbers of $\hat{k}$ on the Ewald sphere can be written as [34]

$$K = 2L^2 + 4 \quad (20)$$

Apparently, the total sampling numbers are enormous, and a great deal of computation resources is needed to perform the translator in the MLFMA.

2) FaFFA ALGORITHM
However, the MLFMA is still expensive for solving the inter-action between large electrical objects and rough surfaces because the translator in the MLFMA is defined on the Ewald sphere with multiple $\hat{k}$ directions. When the group distance is well separated, the translator can be simplified by using the FaFFA, where only a single $\hat{k}$ vector is involved in the translator along the ray-propagation direction. When the group distance kr_{mn} is large enough, the Green function can be simplified as

$$\frac{e^{ik|\boldsymbol{r}_i-\boldsymbol{r}_j|}}{|\boldsymbol{r}_i-\boldsymbol{r}_j|} \sim \frac{e^{ikr_{mn}}}{r_{mn}} e^{ik\hat{r}_{mn}\cdot(\boldsymbol{r}_{im}+\boldsymbol{r}_{nj})} = \frac{ik}{4\pi} \int_{S_E} d^2k e^{ik\hat{k}\cdot(\boldsymbol{r}_{im}+\boldsymbol{r}_{nj})} \alpha_{mn}^{far}$$
$$(21)$$

where

$$\alpha_{mn}^{far} = 4\pi \frac{e^{ikr_{mn}}}{ikr_{mn}} \delta(\hat{k} - \hat{r}_{mn}) \quad (22)$$

Here, we show that only $\hat{k}$ is involved in the FAFFA translator along the ray-propagation direction from group m to group n, as illustrated inEq.(22).

3) COMBINATION OF FaFFA AND MLFMA
In the FaFFA, the far-field condition can be expressed as

$$r_{mn} \ge 3\gamma \sqrt{(D_x^l)^2 + (D_y^l)^2 + (D_z^l)^2} \quad (23)$$

where $3\sqrt{(D_x^l)^2 + (D_y^l)^2 + (D_z^l)^2}$ is the maximum distance of two groups in the second near neighbors [28], and $\gamma \ge 1$. Moreover, the coarsest level L_C should satisfy the condition $L_C > 2$. Thus, when the distance between the source point and the field point satisfies the far-field condition, the FaFFA is used; otherwise, the MLFMA is used. The interactions in the near field area that do not meet the far-field condition are performed with the MLFMA and are defined on the Ewald sphere with many sampling directions. With the distance increasing such that the far-field condition can be satisfied, the translator function is simplified as one sampling direction, where the computing complexity is greatly reduced. An illustration of the MLFMA-FaFFA is shown in Figure. 2. The MLFMA area and the FaFFA area change with changing the distance between the rough surface and the object. When the object is close to the rough surface, the MLFMA area will enlarge, while the FaFFA area will decrease; as a result, the computing time will increase. However, as the distance increases, the MLFMA area will decrease, the FaFFA area will increase, and the computational complexity will decrease correspondingly. Furthermore, when the distance between the facets in the rough surface is very large, its contribution to the mutual interaction is small and could even be ignored. Thus, the very-far facets are discarded to further reduce the computational complexity, and this thought will be discussed next.
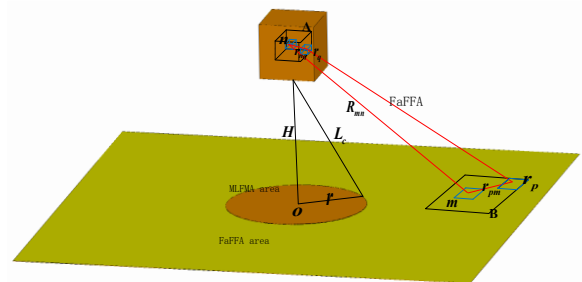

FIGURE 2. Illustration of MLFMA-FaFFA.

B. ADAPTIVE INTEGRAL METHOD(AIM)
Although the impendence matrix $\boldsymbol{Z}_{mn}^{kS}$ is accelerated by the FaFFA, the impedance matrix $[\boldsymbol{Z}_{mn}^{k} + \boldsymbol{Z}_{mn}^{kt} + \boldsymbol{Z}_{mn}^{kS}]$ is still time-consuming, with a computing complexity of $O(M^2)$.

FIGURE 3. Models of truncation for rough surface.

FIGURE 4. Geometry of a rough surface (a)$h_r = 0.1m$, $l_x = l_y = 1.0m$, (b)$h_r = 0.3m$, $l_x = l_y = 1.0m$.

FIGURE 5. Illustration of a single sphere above a rough surface.
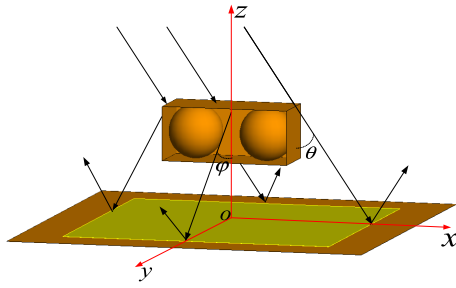
Thus, the adaptive integral method (AIM) is introduced to further accelerate the MoM part. The AIM is used by introducing the auxiliary basis function located on the series of grid nodes [30]. The main process of AIM is shown as follows:

(i). The vector-matrix $\left[\mathbf{Z}_{mn}^{k} + \mathbf{Z}_{mn}^{kt} + \mathbf{Z}_{mn}^{kS}\right]$ is split into the near interaction term $\mathbf{Z}_{mn}^{k}$, which denotes the self-impendence matrix of the object, and the far interaction term $\left[\mathbf{Z}_{mn}^{kt} + \mathbf{Z}_{mn}^{kS}\right]$, which denotes the mutual interaction between different objects and interaction between objects and the rough surface.

(ii). The MoM basis function is projected to the grid points.

(iii). The near interaction term $\mathbf{Z}_{mn}^{k}$ is calculated directly, and the far interaction term $\left[\mathbf{Z}_{mn}^{kt} + \mathbf{Z}_{mn}^{kS}\right]$ is accelerated by FFT.

With the AIM, the computing complexity of the independence matrix in the MoM area is successfully reduced from O(M^2) to O($M \log M$).

C. TRUNCATION FOR ROUGH SURFACE

When computing composite scattering from objects above a rough surface, to fully consider the scattering contribution of a rough surface, the size of the rough surface needs to be large enough. However, as the distances between the rough surface and objects increase, the interaction between them becomes weaker. Thus, it is of great importance to set the proper size of a rough surface to avoid enormous computation for electric currents on rough surfaces and fully consider the interaction between objects and rough surfaces. According to the Kirchhoff approximation, the scattering field in the spectrum reflection direction is the strongest, which is used as the principle for setting the proper size of the rough surface [29].

Suppose that objects are surrounded in a cuboid with length ranges from x_{min} to x_{max}, width ranges from y_{min} to y_{max}, and height ranges from z_{min} to z_{max}. According to the principle of light illumination, the length of the rough surface is

$$x_1 = x_{min} - z_{max} \tan \theta$$
$$x_2 = x_{max} + z_{max} \tan \theta \qquad (24)$$

The width of the rough surface is

$$y_1 = y_{min} - z_{max} \tan \varphi$$
$$y_2 = y_{max} + z_{max} \tan \varphi \qquad (25)$$

where $\theta = \max\{\theta_i, \theta_{s1}, \theta_{s2}, \ldots, \theta_{sn}\}$, and $\varphi = \max\{\varphi_i, \varphi_{s1}, \varphi_{s2}, \ldots, \varphi_{sn}\}$. ($\theta_i, \varphi_i$) is the *i-th* incident angle, and ($\theta_{si}, \varphi_{si}$) is the *i-th* scattering angle.
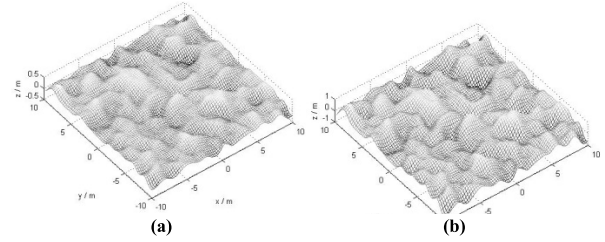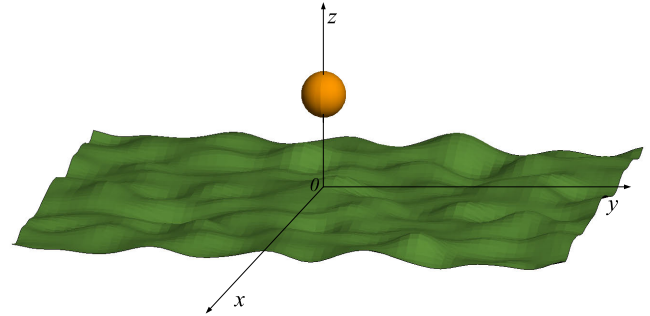
IV. MODEL OF ROUGH SURFACES

In this paper, the rough surface area of S_r^{PO} is simulated by the Gaussian spectrum function [35], and the spectrum function $W\left(K_{xm}, K_{yn}\right)$ can be expressed as

$$W(K_x, K_y) = \frac{l_x l_y h^2}{4\pi} \exp\left(-\frac{K_x^2 l_x^2}{4} - \frac{K_y^2 l_y^2}{4}\right) \qquad (26)$$

where l_x and l_y are the correlation lengths of the rough surface, and h is the root mean square height of the rough surface. Figure 4 presents the geometry of the rough surface.

V. NUMERICAL SIMULATIONS

A. VERIFICATION OF THE IMPROVED MOM-PO

To verify the improved MoM-PO hybrid method, an example of a single conductor sphere above the underlying rough surface is considered, as shown in Figure 5. The calculation parameters are as follows: the working frequency is $f = 0.3$ GHz, the incident angle is $\theta_i = 30°$ and $\varphi_i = 0°$, the observation angle is $\theta_s = -90° \sim 90°$ and $\varphi_s = 0°$, the rough surface type is silt clay, the moisture of silt clay m_v is $0.3 \ g \cdot cm^3$, the environment temperature is 22°C, the relative dielectric constant $\varepsilon = (8.69, -0.47)$, the size of the rough surface is $L_x \times L_y$: $40 \times 40 \ (m^2)$, the root mean square height of the rough surface is $h_{in} 0.1m$, the correlation length of the rough surface is $lx=ly=1 \ m$, five sampling points are considered per wavelength, the size of the perfect conductor sphere is $r^3 = 1 \ m^3$, and the height of the sphere above the underlying surface is H = 5 m. The computing platform is an AMD processor with a speed of 3.2 GHz, a 64-bit kernel and 64 GB RAM. The examples in this paper calculate the statistical average of 30 rough surfaces by the Monte Carlo method.
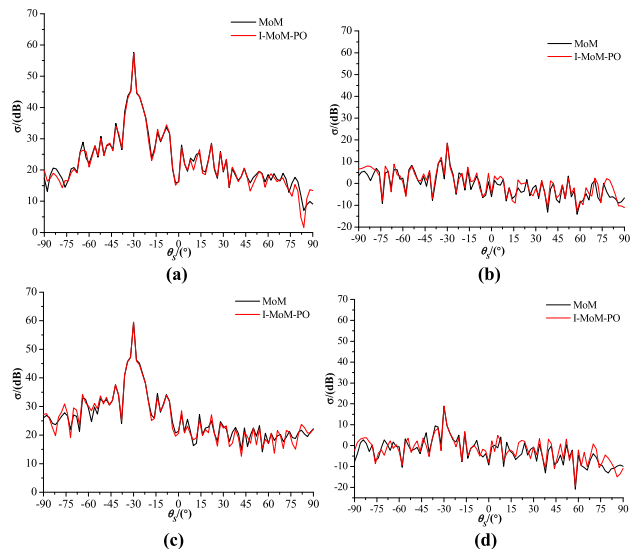
FIGURE 6. Comparison results of four different polarizations obtained by two different solvers: (a) VV polarization, (b) VH polarization, (c) HH polarization, and (d) HV polarization.

The simulation results of the horizontal-horizontal (HH)polarization, vertical-vertical (VV) polarization, horizontal-vertical (HV) polarization and vertical-horizontal (VH) polarization are shown in Figure 6. The proposed method agrees well with the MoM. To better analyze the accuracy of the proposed method, the function of error analysis is used, and the expressions of mean deviation and max deviation are

$$\langle \gamma \rangle = \frac{1}{N_{\theta_s}} \sum_{\{\theta_s\}} |\gamma^T(\theta_s) - \gamma^M(\theta_s)| \qquad (27)$$

$$\max \gamma = \max_{\{\theta_s\}} |\gamma^T(\theta_s) - \gamma^M(\theta_s)| \qquad (28)$$

where $\gamma^T(\theta_s)$ is the BCS obtained by improved MoM-PO, $\gamma^M(\theta_s)$ is the BCS obtained by the MoM, and N_{θ_s} is the number of scattering angles.

TABLE 1. Error analysis for different polarizations.

Polarizations	$\langle \gamma \rangle$ /dB	max γ /dB
VV	1.1563	4.9219
HH	1.3020	4.4732
VH	1.8644	6.5717
HV	1.9777	6.2565

The comparison results are shown in TABLE 1. In VV and HH polarizations, this proposed method agrees well with the MoM under the PO condition. In VH and HVpolarizations, the accuracy of the proposed method is not satisfactory. The reason for this is that the proposed method has not considered the coupling interaction between different facets on the rough surface.

The simulation results obtained for different root mean square (RMS) values are shown in Fig. 7. The calculation

parameters are the same as those in Figure 6 except for the RMS height. The RMS heights are $h_{in} = 0.1 \ \lambda \ and$ $h_{in} = 0.3 \ \lambda$. With increasing RMS, the BCS in the specular direction decreases, and the BCS in the backward scattering direction increases. The reason is that the BCSs in the specular direction are mostly caused by coherent scattering, while the BCSs in the backward scattering direction are mostly caused by incoherent scattering. Thus, with increasing RMS, coherent scattering becomes weak, and incoherent scattering becomes stronger, which results in weak BCSs in the specular direction and stronger BCSs in the backward scattering direction.
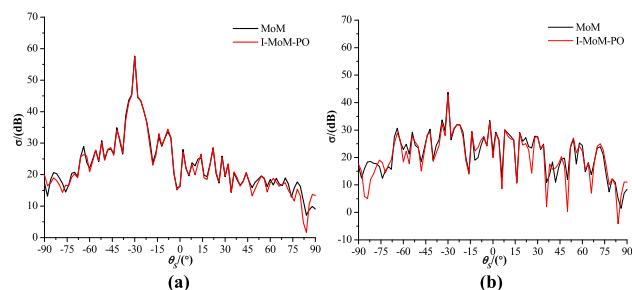

FIGURE 7. Comparison results obtained for different RMS values by two different solvers: (a) $h_{in} = 0.1\lambda$ *and* (b) $h_{in} = 0.3\lambda$.

The different results are compared in TABLE 2. As the RMS increases, the accuracy of the imposed method worsens, especially at large incident angles. The reason for this lies in that the mutual interaction becomes stronger when the RMS increases and the imposed method ignores it. These results show that this proposed method has limitations, especially for rough surfaces with large RMS heights. Thus, this method is suitable for composite scattering from complex targets above a surface with a small RMS.

TABLE 2. Error analysis for different RMS.

RMS/λ	$\langle \gamma \rangle$ /dB	max γ /dB
0.1	1.1563	4.9219
0.3	2.3079	11.3415

The computational times and storage requirements for the two solvers are compared in Table 3. The storage requirement of the improved MoM-PO is 0.12% of that of MoM, and the computation time of the improved MoM-PO is 2.3% of that of the MoM. This result shows that the improved MoM-PO technique has a low storage requirement and high efficiency.

B. COMPOSITE SCATTERING FROM DIFFERENT QUANTITIES OF OBJECTS ABOVE A ROUGH SURFACE

A comparison of the results obtained for the BCS from one, two, and three cubes above a rough surface is presented in Figure 7. The size of the cubes is $l \times l \times l$: $2 \times 2 \times 2 \ (m^3)$, the incident angle is $\theta_i = 30°$ and $\varphi_i = 0°$, the observation angle is $\theta_s = -90° \sim 90°$ and $\varphi_s = 0°$, the rough surface is silt clay, the moisture content of silt clay m_v is $= 0.3$ $g \cdot cm^3$, and the relative dielectric constant $\varepsilon = (8.69, -0.47)$.
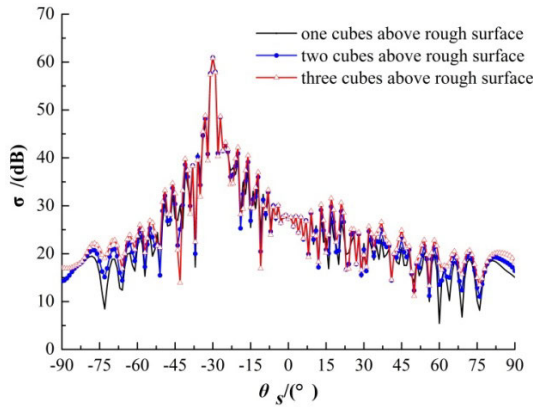
FIGURE 8. Bistatic scattering coefficient (BCS) obtained for different numbers of objects.

TABLE 3. Comparison of the computation results and storage requirement by three solvers.

Polarization model	Method	Computation time/s	Storage requirement/Gbyte
VV	MoM	102142	63.595
	I-MoM-PO	1641	0.853
HH	MoM	100525	63.595
	I-MoM-PO	1610	0.853

It is observed that BCS increases with increasing numbers of targets. Moreover, the BCS values obtained for the cubes with different numbers of targets above the rough surface are the same in the mirror scattering direction, and the difference between the BCS values for the cubes with different numbers of targets increases with increasing scattering angles. This finding is because the mutual interaction between the targets and the underlying rough surface has little influence on mirror scattering, while in the other directions, the BCS increases with the increasing numbers of targets.

C. COMPOSITESCATTERING FROM OBJECTS ABOVE A ROUGH SURFACE WITH DIFFERENT INCIDENT ANGLES

The composite scattering models for the cubes above a silt clay surface with different incident angles are shown in Figure 9. The comparison of the obtained BCS with different incident angles is presented in Figure 10. The incident angles are $\theta_i = 30°$ and $\varphi_i = 0°$, $\theta_i = 30°$ and $\varphi_i = 45°$ and $\theta_i = 30°$ and $\varphi_i = 90°$, and the observation angles are $\theta_s = -90° \sim 90°$ and $\varphi_s = 0°$, $\theta_s = -90° \sim 90°$ and $\varphi_s = 45°$ and $\theta_s = -90° \sim 90°$ and $\varphi_s = 90°$; the size of the cubes is $l \times l \times l$: $2 \times 2 \times 2$ m³, the rough surface is silt clay, the moisture content of silt clay m_v is $= 0.3$ $g \cdot cm^3$, and the relative dielectric constant $\varepsilon = (8.69, -0.47)$. It is observed that the BCS from the cubes above silt clay with the incident angle of $\theta_i = 30°$ and $\varphi_i = 0°$ is the largest among the values obtained for the three incident angles. The fluctuation of the BCS from the cubes above silt clay is larger for the incident angle of $\theta_i = 30°$ and $\varphi_i = 45°$ than that for the incident angles of $\theta_i = 30°$ and $\varphi_i = 0°$ and $\theta_i = 30°$ and $\varphi_i = 90°$. This finding is
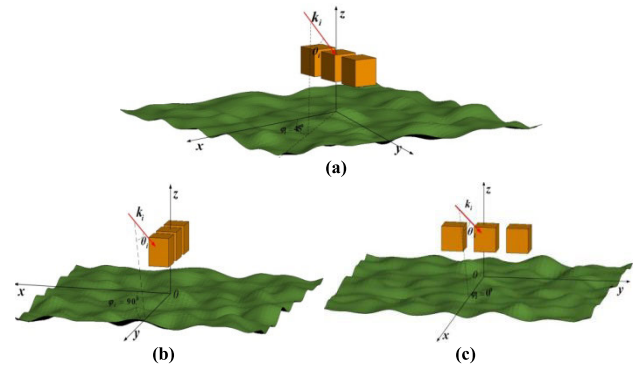

FIGURE 9. Models of composite scattering from cubes above a rough surface with different incident angles: (a) incident angle is $\theta_i = 30°$ and $\varphi_i = 0°$; (b) incident angle is $\theta_i = 30°$ and $\varphi_i = 45°$; (c) incident angle is $\theta_i = 30°$ and $\varphi_i = 90°$.
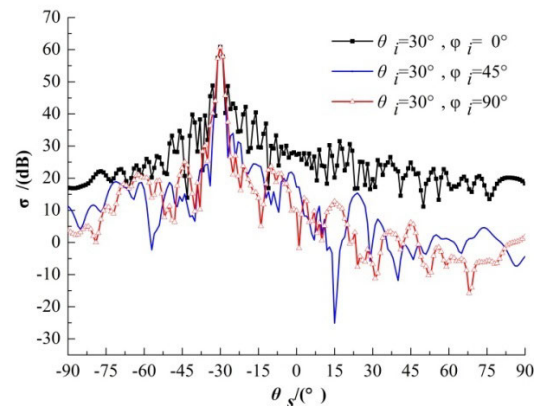

FIGURE 10. Bistatic scattering coefficient (BCS) obtained for different incident angles.

because the illuminated area is larger for the incident angle of $\theta_i = 30°$ and $\varphi_i = 0°$ and because scattering from an edge is stronger for the incident angle of $\theta_i = 30°$ and $\varphi_i = 45°$.

D. COMPOSITE SCATTERING FROM OBJECTS WITH DIFFERENT LOCATIONS ABOVE A ROUGH SURFACE

The model of the cubes with different positions above the rough surface is shown in Figure 11. The BCS results obtained for the three cubes parallel to the rough surface and for the three cubes rotated by 45° relative to the rough surface are compared in Figure 12. The three cubes are located above the rough surface and are parallel to and rotated by 45° with respect to the rough surface; the incident angle is $\theta_i = 30°$ and $\varphi_i = 0°$, the observation angle is $\theta_s = -90° \sim 90°$ and $\varphi_s = 0°$, the size of the cubes is $l \times l \times l$: $2 \times 2 \times 2$ m³, the rough surface is silt clay, the moisture of the soil m_v is $= 0.3$ $g \cdot cm^3$, and the relative dielectric constant $\varepsilon = (8.69, -0.47)$. The mirror scattering from the two different positions is the same, and the backward scattering from the three cubes parallel to the rough surface is stronger than that for the three cubes rotated by 45° with respect to the rough surface. However, for the composite model in the large scattering angle directions, the BCS obtained for the cubes rotated by 45° with respect
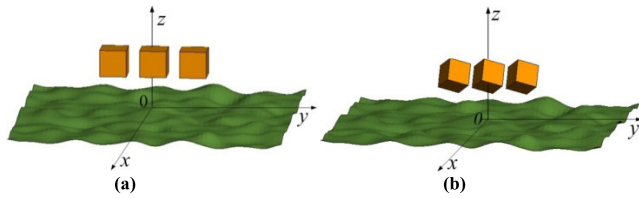
FIGURE 11. Models of composite scattering for cubes with different positions above a rough surface: (a) three cubes parallel to the rough surface and (b) three cubes rotated 45° with respect to the rough surface.
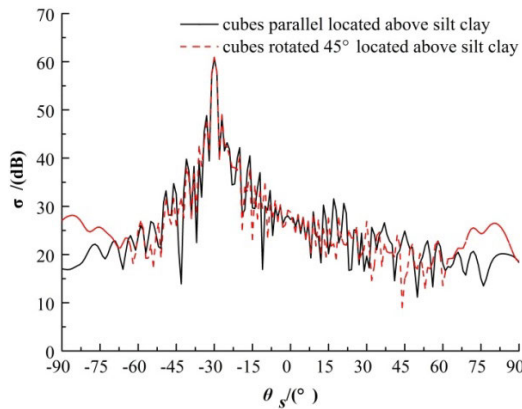

FIGURE 12. Bistatic scattering coefficient (BCS) obtained for different positions of the objects.

FIGURE 13. Models of composite scattering for cubes with different types above a rough surface: (a) three spheres above a rough surface, (b) three cylinders above a rough surface, and (c) three cubes above a rough surface.

FIGURE 14. Bistatic scattering coefficient (BCS) obtained for different types of objects.

to the roughness is higher than that for three cubes parallel to the rough surface. This result is because the contact area between the cubes and the rough surface is larger when the cubes are parallel to the rough surface, contributing to the increased mutual interaction between the cubes and the rough surface. Due to scattering from the edge of the cubes, the BCS obtained from the cubes rotated by 45° with respect to the rough surface is larger in the large scattering angle directions.

E. COMPOSITE SCATTERING FROM DIFFERENT TYPES OF OBJECTS ABOVE ROUGH SURFACE

The model of composite scattering from different types of targets above the rough surface is shown in Figure 13. The BCS results obtained for the three different types of targets above a rough surface are compared in Figure 14. The targets are spheres, cylinders and cubes, the incident angle is $\theta_i = 30°$ and $\varphi_i = 0°$, the observation angle is $\theta_s = -90° \sim 90°$ and $\varphi_s = 0°$, the size of the cubes is $l \times l \times l$: $2 \times 2 \times 2$ m^3, the size of the cylinders is $\pi r^2 \times l$: $\pi \times 1^2 \times 2$ m^3, the size of the spheres is $4/3\pi r^3$: $4/3\pi \times 1^2$ m^3, the rough surface is silt clay, the moisture of the soil m_v is $= 0.3$ $g \cdot cm^3$, and the relative dielectric constant is $\varepsilon = (8.69, -0.47)$. It is observed that the highest BCS values are obtained for the three cubes above a rough surface and that the BCS obtained for the three spheres above a rough surface are the lowest. Moreover, both in the mirror scattering direction and in the backward scattering direction, the BCS obtained for the cubes above a rough surface are higher than those obtained for the spheres and cylinders. This result is because the cubes have more
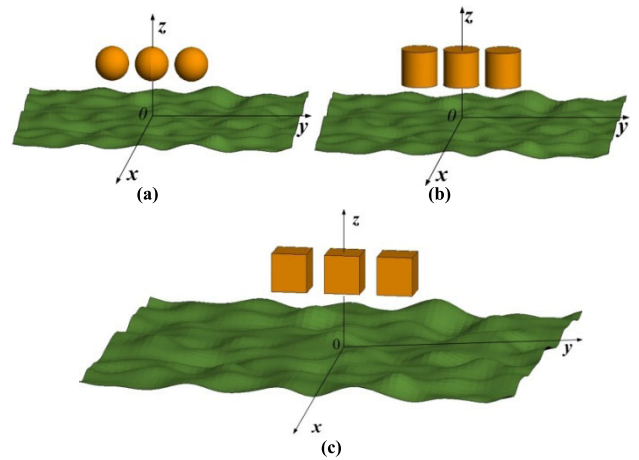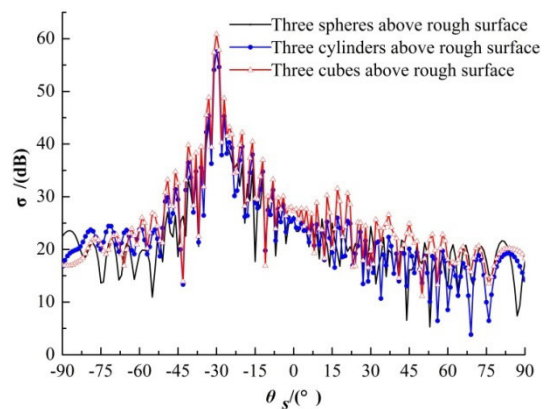
edges than either the cylinders or spheres, leading to stronger interactions between cubes and rough surfaces.

F. COMPOSITE SCATTERING FROM OBJECTS ABOVE DIFFERENT TYPES OF ROUGH SURFACE

The BCS values obtained for three cubes above three different types of rough surfaces are compared in Figure 15. The rough surface types are sandy soils, silt loam and silt clay, and the relative dielectric constants of sandy soils, silt loam and silt clay are $\varepsilon = (15.10, -0.91)$, $\varepsilon = (13.61, -0.79)$, and $\varepsilon = (8.69, -0.47)$, respectively. The incident angle is $\theta_i = 30°$ and $\varphi_i = 0°$, the observation angle is $\theta_s = -90° \sim 90°$ and $\varphi_s = 0°$, the size of the cubes is $l \times l \times l$: $2 \times 2 \times 2$ m^3, and the soil moisture m_v is $= 0.3$ $g \cdot cm^3$. It is observed that the BCS values obtained for the cubes above the sandy soils are higher than those obtained for the other soil types. Moreover, in the mirror scattering direction, the BCS values obtained for the cubes above the sandy soil are higher than those obtained for cubes above silt loam and silt clay. This result is because the relative dielectric constant of sandy soils is higher than that of
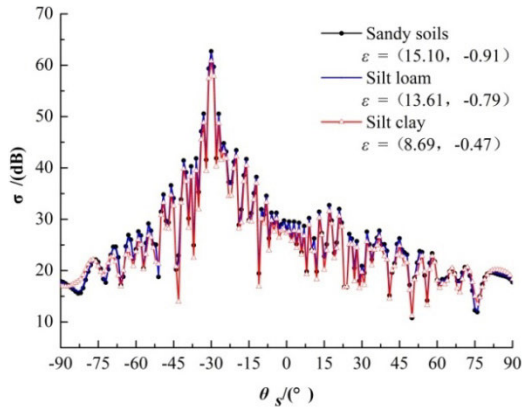
FIGURE 15. Bistatic scattering coefficient (BCS) obtained with different types of soil.
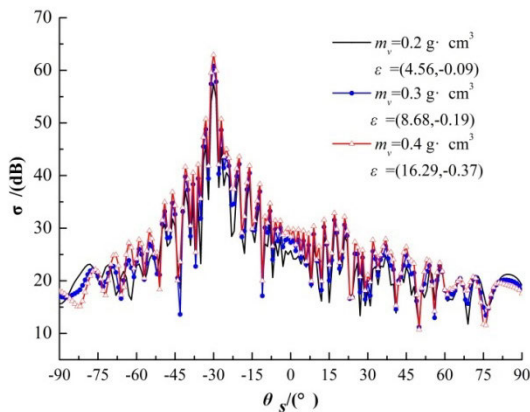

FIGURE 16. Bistatic scattering coefficient (BCS) obtained for different soil moisture contents.

silt loam and silt clay, leading to a stronger reflection effect for sandy soils and a stronger interaction between the cubes and sandy soils.

G. COMPOSITE SCATTERING FROM OBJECTS ABOVE A ROUGH SURFACE WITH DIFFERENT MOISTURE CONTENTS OF THE SOIL

The BCS values obtained for three cubes above silt clay with different moisture contents are compared in Figure 16. The rough surface is silt clay, the moisture contents of silt clay are $m_v = 0.2$ $g \cdot cm^3$, $m_v = 0.3$ $g \cdot cm^3$, and $m_v = 0.4$ $g \cdot cm^3$, and the relative dielectric constants of silt clay with three different moisture contents are $\varepsilon = (4.56, 0.09)$, $\varepsilon = (8.68, 0.19)$, and $\varepsilon = (16.29, 0.37)$. The incident angle is $\theta_i = 30°$ and $\varphi_i = 0°$, the observation angle is $\theta_s = -90° \sim 90°$ and $\varphi_s = 0°$, and the size of the cubes is $l \times l \times l$: $2 \times 2 \times 2$ m^3. It is observed that as the moisture content of the rough surface increases, the real part of the relative dielectric constant increases strongly, and the imaginary part of the relative dielectric constant decreases slightly. Thus, the BCS values obtained for the cubes above silt clay with a moisture content m_v of $= 0.4$ $g \cdot cm^3$ are the highest. Moreover, the BCS obtained for the cubes above the silt clay increases both in the mirror scattering direction and

in the backward scattering direction with increasing moisture content. This result is because the relative dielectric constant increases with increasing moisture content, contributing to the increasing reflection effects of silt clay and the increase in the interaction between the cubes and the silt clay rough surface.

VI. CONCLUSION

To solve scattering from multiple 3D conducting objects above a 2D random electrically large rough dielectric surface, an improved hybrid method combining the method of moment and the physical optics method is proposed in this paper. The contribution of the PO area and interactions of different objects are coupled into the independence matrix equation of the MoM part. In the coupled MoM-PO technique, computation of the interactions between objects and rough surfaces and solving for the impedance matrix equation are two problems. To solve the computational bottleneck, accelerating techniques are adopted. First, the combined multilevel fast multipole algorithms and fast far field approximation (MLFMA-FaFFA) are used to accelerate the matrix vector multiplications between objects and rough surfaces. The rough surface truncation technique is applied to further reduce computation complexity. In addition, the adaptive integral method (AIM) is applied to solve the impedance matrix equations of the MoM part. Compared with traditional MoM-PO, this improved hybrid method is proven to be much faster and maintain the same accuracy. Finally, the BCSs obtained for multiple objects above a random dielectric rough surface under different conditions are analyzed and discussed in detail. Our future study will address composite scattering from multiple dielectric objects above a random dielectric rough surface by the improved MoM-PO method.

REFERENCES

[1] N. M. Estakhri, B. Edwards, and N. Engheta, "Inverse-designed metastructures that solve equations," *Science*, vol. 363, no. 6433, pp. 1333–1338, Mar. 2019.

[2] L. La Spada and L. Vegni, "Near-zero-index wires," *Opt. Exp.*, vol. 25, no. 20, pp. 23699–23708, Oct. 2017.

[3] N. J. Greybush, V. Pacheco-Peña, N. Engheta, C. B. Murray, and C. R. Kagan, "Plasmonic optical and chiroptical response of self-assembled Au nanorod equilateral trimers," *ACS Nano*, vol. 13, no. 2, pp. 1617–1624, 2019.

[4] L. L. Spada, C. Spooner, S. Haq, and Y. Hao, "Curvilinear metasurfaces for surface wave manipulation," *Sci. Rep.*, vol. 9, no. 1, p. 3107, 2019.

[5] I.-H. Lee, D. Yoo, P. Avouris, T. Low, and S.-H. Oh, "Graphene acoustic plasmon resonator for ultrasensitive infrared spectroscopy," *Nature Nanotechnol.*, vol. 14, no. 4, pp. 313–319, Apr. 2019.

[6] L. La Spada and L. Vegni, "Electromagnetic nanoparticles for sensing and medical diagnostic applications," *Materials*, vol. 11, no. 4, p. 603, Apr. 2018.

[7] Y. Liang, L. Guo, and Z. Wu, "The EPILE combined with the generalized-FBM for analyzing the scattering from targets above and on a rough surface," *IEEE Antennas Wireless Propag. Lett.*, vol. 9, pp. 809–813, 2010.

[8] Y. Liang, L.-X. Guo, and Z.-S. Wu, "The fast EPILE combined with FBM for electromagnetic scattering from dielectric targets above and below the dielectric rough surface," *IEEE Trans. Geosci. Remote Sens.*, vol. 49, no. 10, pp. 3892–3905, Oct. 2011.

[9] X. C. Ren, X. M. Zhu, and P. Liu, "Wide-band composite electromagnetic scattering from the earth soil surface and multiple targets shallowly buried," *Acta Phys. Sinica*, vol. 65, no. 20, 2016, Art. no. 204101.

[10] L. Bing, M. Meng-Chen, and L. Ming-Zhu, "Hybrid algorithm for composite electromagnetic scattering from the multi-target on and above rough sea surface," *Acta Phys. Sinica*, vol. 66, no. 5, 2017, Art. no. 050301.

[11] X. Wang, Y.-B. Gan, and L.-W. Li, "Electromagnetic scattering by partially buried PEC cylinder at the dielectric rough surface interface: TM case," *IEEE Antennas Wireless Propag. Lett.*, vol. 2, pp. 319–322, 2003.

[12] M. R. Hestenes and E. Stiefel, "Methods of conjugate gradients for solving linear systems," *J. Res. Nat. Bur. Standards*, vol. 49, no. 6, pp. 409–436. 1952.

[13] N. Déchamps, N. De Beaucoudrey, C. Bourlier, and S. Toutain, "Fast numerical method for electromagnetic scattering by rough layered interfaces: Propagation-inside-layer expansion method," *J. Opt. Soc. Amer. A, Opt. Image Sci.*, vol. 23, no. 2, pp. 359–369, 2006.

[14] S. Bellez, C. Bourlier, and G. Kubické, "3-D scattering from a PEC target buried beneath a dielectric rough surface: An efficient PILE-ACA algorithm for solving a hybrid KA-EFIE formulation," *IEEE Trans. Antennas Propag.*, vol. 63, no. 11, pp. 5003–5014, Nov. 2015.

[15] M. R. Pino, L. Landesa, J. L. Rodriguez, F. Obelleiro, and R. J. Burkholder, "The generalized forward-backward method for analyzing the scattering from targets on ocean-like rough surfaces," *IEEE Trans. Antennas Propag.*, vol. 47, no. 6, pp. 961–969, Jun. 1999.

[16] M. El-Shenawee and C. M. Rappaport, "Monte Carlo simulations for clutter statistics in minefields: AP-mine-like-target buried near a dielectric object beneath 2-D random rough ground surfaces," *IEEE Trans. Geosci. Remote Sens.*, vol. 40, no. 6, pp. 1416–1426, Jun. 2002.

[17] C. Shui-Rong and G. Li-Xin, "A new fast algorithm based on compressive sensing for composite electromagnetic back scattering from a 2D ship located on a 1D rough sea surface," *Acta Phys. Sinica*, vol. 64, no. 6, 2015, Art. no. 060301.

[18] K. Xu, D. Z. Ding, Z. H. Fan, and R. S. Chen, "Multilevel fast multipole algorithm enhanced by GPU parallel technique for electromagnetic scattering problems," *Microw. Opt. Technol. Lett.*, vol. 52, no. 3, pp. 502–507, Mar. 2010.

[19] J. Li, L.-X. Guo, S.-R. Chai, and Y.-C. Jiao, "Electromagnetic scattering from a PEC object above a dielectric rough sea surface by a hybrid PO–PO method," *Waves Random Complex Media*, vol. 25, no. 1, pp. 60–74, Jan. 2015.

[20] R. Wang, L. X. Guo, S. T. Qin, and Z. S. Wu, "Hybrid method for investigation of electromagnetic scattering interaction between the conducting target and rough sea surface," *Phys. Sinica*, vol. 57, no. 6, pp. 3474–3480, 2008.

[21] Y. Zhang, Y. E. Yang, H. Braunisch, and J. A. Kong, "Electromagnetic wave interaction of conducting object with rough surface by hybrid SPM/MOM technique," *Prog. Electromagn. Res.*, vol. 22, pp. 315–335, 1999.

[22] J. Li, L. X. Guo, and Q. He, "Hybrid FE-BI-KA method in analysing scattering from dielectric object above sea surface," *Electron. Lett.*, vol. 47, pp. 1147–1148, Sep. 2011.

[23] J. Li, K. Li, L.-X. Guo, and Z.-Y. Liu, "A hybrid IEM–PO method for composite scattering from a PEC object above a dielectric sea surface with large windspeed: HH polarization," *Waves Random Complex Media*, vol. 28, no. 4, pp. 630–642, Oct. 2018.

[24] H. X. Ye and Y. Q. Jin, "A hybrid analytical-numerical algorithm for computation of scattering from a 3D PEC target above a dielectric rough surface," *Chin. J. Radio Sci.*, vol. 23, no. 6, pp. 1144–1187, 2008.

[25] T. Wei, R. Xin-Cheng, and G. Li-Xin, "Study on composite electromagnetic scattering from the double rectangular cross-section columns above rough sea surface using hybrid method," *Acta Phys. Sinica*, vol. 64, no. 17, 2015, Art. no. 174101.

[26] C. C. Lu and W. C. Chew, "Fast far-field approximation for calculating the RCS of large objects," *Microw. Opt. Tech. Lett.*, vol. 8, pp. 238–241, Apr. 1995.

[27] G. Tian, C. Ming Tong, H. Liu, and P. Peng, "An improved MoM-PO hybrid method for scattering from multiple 3-D objects above the 2-D random conducting rough surface," *Electromagnetics*, vol. 39, no. 5, pp. 375–392, Jul. 2019.

[28] W. Cho Chew, T. Jun Cui, and J. M. Song, "A FAFFA-MLFMA algorithm for electromagnetic scattering," *IEEE Trans. Antennas Propag.*, vol. 50, no. 11, pp. 1641–1649, Nov. 2002.

[29] X. Y. Zhang and X. Q. Sheng, "Method for computing the backscattering from objects above a dielectric rough surface," *Trans. Beijing Inst. Technol.*, vol. 30, no. 4, pp. 460–463, 2010.

[30] C.-F. Wang, F. Ling, J. Song, and J.-M. Jin, "Adaptive integral solution of combined field integral equation," *Microw. Opt. Technol. Lett.*, vol. 19, no. 5, pp. 321–328, Dec. 1998.

[31] Z.-L. Liu and C.-F. Wang, "Efficient iterative method of moments—Physical optics hybrid technique for electrically large objects," *IEEE Trans. Antennas Propag.*, vol. 60, no. 7, pp. 3520–3525, Jul. 2012.

[32] R. Coifman, V. Rokhlin, and S. Wandzura, "The fast multipole method for the wave equation: A pedestrian prescription," *IEEE Antennas Propag. Mag.*, vol. 35, no. 3, pp. 7–12, Jun. 1993.

[33] W. C. Chew, E. Michielssen, J. M. Song, and J. M. Jin, *Fast and Efficient Algorithms in Computational Electromagnetics*. New York, NY, USA: Artech House, 2001.

[34] J. Song, C. C. Lu, and W. C. Chew, "Multilevel fast multipole algorithm for electromagnetic scattering by large complex objects," *IEEE Trans. Antennas Propag.*, vol. 45, pp. 1488–1493, 1997.

[35] C. Bourlier, G. Berginc, and J. Saillard, "Theoretical study on two-dimensional Gaussian rough sea surface emission and reflection in the infrared frequencies with shadowing effect," *IEEE Trans. Geosci. Remote Sens.*, vol. 39, no. 2, pp. 379–392, Feb. 2001.

[36] R. Wang, L. X. Guo, and A. Q. Wang, "Investigation of electromagnetic scattering interaction between the buried target and the rough surface in different types of soil," *Acta Phys. Sinica*, vol. 59, no. 5, pp. 3179–3186, 2010.

[37] L. Tsang, J. A. Kong, and K. H. Ding, *Scattering of Electromagnetic Waves: Numerical Simulations*. New York, NY, USA: Wiley, 2000, pp. 278–285 and 565–571.

GUILONG TIAN was born in Hunan, China, in 1994. He received the B.S. degree in electronics science and technology and the M.S. degree in electromagnetic theory and engineering from Air Force Engineering University, Xi'an, China, in 2012 and 2016, respectively, where he is currently pursuing the Ph.D. degree in electronics science and technology. His research interests include computational electromagnetics and composite scattering from objects above rough surface.

CHUANGMING TONG was a Visiting Scientist Postdoctoral Fellow with Southeast University, Nanjing, China. He is currently a Professor with the Department of Electronics and Communication Engineering, Air and Missile Defense College, Air Force Engineering University. He has more than 20 years of experience in teaching and research. His research interests include microwave remote sensing, electromagnetic waves, polarimetric and interferometric applications of microwave data, and numerical modeling, ground penetrating radar, through wall imaging, and stealth technology. He received various fellowships and awards from national and international bodies.
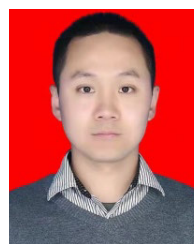
HUALONG SUN was born in Shaanxi, China, in April 1982. He received the M.S. degree in radio engineering from Southeast University, Nanjing, China, and the Ph.D. degree in electronic science and technology from Air Force Engineering University, Xi'an, China, in 2007 and 2017, respectively. His main research interests include electromagnetic scattering, computational electromagnetic, and antenna design.

GAOXIANG ZOU was born in Hunan, China, in 1993. He received the B.S. degree in radar engineering and the M.S. degree in electronics science and technology from Air Force Engineering University, Xi'an, China, in 2015 and 2018, respectively, where he is currently pursuing the Ph.D. degree in electromagnetic theory and engineering.

His research interests include computational electromagnetism, Brewster effect, multipath effect, modeling theory of divisional environments, and electromagnetic scattering characteristics of composite targets above divisional environments.

HAO LIU was born in Shangdong, China, in 1990. He received the B.S. degree in radar engineering from Air Force Engineering University, Xi'an, China, in 2010, and the M.S. degree in electromagnetic theory and engineering from Strategic Support Force Aerospace Engineering University, Beijing, China, in 2016. His research interests include computational electromagnetics and wave scattering from rough surface.

• • •